Acta Materialia 202 (2021) 68–79

Contents lists available at ScienceDirect

Acta Materialia

journal homepage: www.elsevier.com/locate/actamat

Local slip resistances in equal-molar MoNbTi multi-principal element alloy

Shuozhi Xu[a,*], Yanqing Su[b], Wu-Rong Jian[b], Irene J. Beyerlein[a,b,c,1]

[a] California NanoSystems Institute, University of California, Santa Barbara, Santa Barbara CA 93106-6105, USA
[b] Department of Mechanical Engineering, University of California, Santa Barbara, Santa Barbara CA 93106-5070, USA
[c] Materials Department, University of California, Santa Barbara, Santa Barbara CA 93106-5050, USA

ARTICLE INFO

Article history:
Received 8 July 2020
Revised 16 October 2020
Accepted 18 October 2020
Available online 21 October 2020

Keywords:
Local slip resistance
Peierls stress
Multi-principal element alloys
Body-centered cubic metals
Molecular statics

ABSTRACT

In this work, we calculate the local slip resistances (LSRs) in equal-molar MoNbTi multi-principal element alloy via molecular static simulations. We consider dislocations of either screw or edge character gliding on four types of slip planes, {110}, {112}, {123}, and {134}, in either forward or backward sense of the 111 slip direction. As references, we also compute the Peierls stresses of the same dislocations in two natural reference metals, Mo and Nb, and a synthetic one, the mean-field, *A*-atom potential-based MoNbTi. Further, we compare the LSRs with the corresponding ideal shear strengths that do not account for the lattice distortions induced by dislocation cores. We show that for neither dislocation character is the LSR on the {110} plane the lowest in MoNbTi, in contrast to Mo and Nb. For edge dislocations, slip on the {134} plane is the easiest, but for the screw dislocations, it is the hardest. For screw dislocations, the {112} glide plane is the most favored, while for edge dislocations, it is the least favored. We also find that the screw-to-edge ratio in the slip resistance is reduced by one order of magnitude in MoNbTi compared to that of any pure reference metal for the same type of slip plane. These results suggest that, in contrast to pure body-centered cubic (BCC) metals, BCC MPEAs could deform by a multiplicity of slip modes due to the lower screw-to-edge ratios and the lower LSRs for edge dislocations on the three higher order planes.

1. Introduction

Multi-principal element alloys (MPEAs) are alloys that form solid solution phases and consist of three or more principal metallic elements [1,2]. Improving the structural integrity of MPEAs requires knowledge of their plastic deformation. Due to the similarity in the underlying body-centered cubic (BCC) lattice between pure metals and MPEAs, plasticity in both types of crystals is primarily caused by dislocation slip [3]. Therefore, knowledge of dislocation motion and processes, such as the critical activation stresses and preferred glide planes, is valuable for understanding the plastic response of MPEAs.

In pure metals, the Peierls stress is a good measure of the critical resolved shear stress for a straight dislocation line to glide in an otherwise defect-free infinite crystal. Peierls [4] defined a peak energetic barrier for a straight dislocation to move from one lattice point to another and from the associated work done, a threshold stress, or Peierls stress, can be determined. By definition, the Peierls stress is invariant with respect to the dislocation length and the location at which the dislocation lies. As long as there are no other nearby defects or surfaces, stresses exceeding the Peierls stress are, in principle, deemed sufficient for continued glide of the dislocation [5].

Dislocations in pure BCC metals exhibit many characteristics that are not usually seen in metals with the other common cubic structure: face-centered cubic (FCC) [6,7]. In BCC metals, dislocations glide on multiple glide planes, such as {110}, {112}, and {123}, sharing the same Burgers vector $(a_0/2)\langle 111\rangle$, where a_0 is the lattice parameter [8]. The {112} glide planes, in particular, are known to have a twinning/anti-twinning asymmetry [9]. This asymmetry in twinning was shown to result in asymmetry in the Peierls stress, of both edge [10,11] and screw [12,13] dislocations. In the same BCC metal, on the same glide plane, the Peierls stress of the screw dislocation is usually much higher than those of the non-screw ones. Among four BCC refractory metals — Mo, Nb, Ta, and W — the slip resistance of a screw dislocation on {110} plane at a few K has been estimated to be 18–31 times higher than those of an edge dislocation on the same plane in the same metal [14].

* Corresponding author.
E-mail address: shuozhixu@ucsb.edu (S. Xu).

[1] Irene J. Beyerlein was an Editor of the journal during the review period of the article. To avoid a conflict of interest, Irene J. Beyerlein was blinded to the record and another editor processed this manuscript.

https://doi.org/10.1016/j.actamat.2020.10.042
1359-6454/

Consequently, the plasticity of BCC pure metals at low temperatures is mainly controlled by the glide of screw dislocations, which move by kink-pair formation and migration and not by simultaneous motion of an entire line [15]. Last, the screw dislocations in BCC metals can display a non-Schmid response, wherein their glide is influenced by non-resolved-shear-stress components [16,17].

Unlike pure metals, MPEAs have atomic-scale fluctuations in chemical compositions that lead to sluggish diffusion [18] and severe lattice distortion [19]. In many recent studies, the question has been raised on whether the conventional understanding of dislocation glide based on single-element metals could be translated to MPEAs. Recently, it was observed in experiments and atomistic simulations that both edge and screw dislocations can play an important role in the plasticity of BCC MPEAs. For example, in $NbTi_2Zr$ and NbTiZr MPEAs, respectively, the ratios in the mobility between the edge and screw dislocations are found to be 6.3 by experiments [20] and 2 by molecular dynamics (MD) simulations [21]. The ratio in $Co_{16.67}Fe_{36.67}Ni_{16.67}Ti_{30}$ MPEAs was estimated by MD simulations to be 1.1–1.2 [22]. Likewise, in MoNbTaW MPEAs, using MD calculations at a few K, the ratio was found to be 2.76 [14]. Note that all these investigations only considered slips on {110} planes.

On the one hand, dislocation motion is mostly affected by the atoms inside and in the vicinity of the dislocation core. On the other hand, the atomic-scale compositional fluctuations in MPEAs can lead to frequent variation in the atomic type in the region a dislocation may glide through. Consequently, unlike in a pure metal, the critical stress for a short dislocation to glide in an MPEA depends on the position of the dislocation. To compare the critical stress in MPEAs with the Peierls stress in pure metals, analogous definitions have been proposed. Some modeling studies, e.g., those in MoNbTaW MPEAs, retained the names “Peierls stress” [14] and “Peierls barrier” [23] to describe respectively, the critical stress and energy barrier for a short screw dislocation (0.6–2.2 nm) to move by a short distance ($\approx$ 0.4 nm). Maresca and Curtin [24] proposed that the energy barrier for a long screw dislocation in MPEAs to move from one energy valley to another at low temperatures equals the intrinsic Peierls barrier plus the barrier created by the solute potential energy minus any annihilation of kinks. In a recent paper, molecular static (MS) calculations were employed to calculate the critical stress to move a short, straight dislocation in MoNbTi [25]. The resulting critical stress to glide was referred to as the local slip resistance (LSR). Unlike in a pure metal, in which the Peierls stress is deterministic, the LSR varies statistically with the dislocation’s location in the plane and from plane to plane. Like the Peierls stress, the LSR is associated with a short dislocation segment of characteristic length that remains straight as it moves, unlike long dislocations that can assume a wavy morphology. This unit strength aptly assesses the effect of the local chemical variation and atomically distorted environment on the slip resistance separate from line tension. Recently, it was reported that the LSR for glide on the {110} plane can vary significantly among parallel planes in manynominally random BCC MPEAs [26,27]. A similar model with a short dislocation line length ($\approx$ 0.6 nm) was recently employed to study the effects of the short-range order on dislocation core energy in MoNbTaW [23].

Most prior *ab initio* [23] and atomistic simulations [21,22,24,28,29] in BCC MPEAs have primarily focused on glide in the $\{110\}\langle 111\rangle$ family. Yet even in pure BCC metals, slip on planes with higher orders can be as prevalent as those on {110} planes [30]. Take MS calculations in Fe as an example. A wide range of Peierls stresses, even for the same type of dislocation on the same type of slip plane, were reported as a result of the different interatomic potentials used. Peierls stresses of an edge dislocation are 25–322 MPa on the {110} plane, [31–33], 129–805 MPa on the {112} plane [10,34], and 25–550 MPa on the {123} plane [35]. Peierls stresses of a screw dislocation are generally much higher: 900–2334 MPa on the {110} plane [36–39], 1771–5715 MPa on the {112} plane [36], and 900–2100 MPa on the {123} plane [35]. Recent experimental results on MoNbTi identified that dislocation slips on the higher order planes, including {112}, {123} and {134}, play a more important role in plastic deformation than that on the {110} planes [25].

In this work, we analyze the LSR values on {110}, {112}, {123} and {134} planes in the equal-molar MoNbTi MPEA. We compare the mean and standard deviation of LSR across different types of slip planes, correlate all LSR values with newly calculated ideal shear strengths, and identify the effects of compositional fluctuation and lattice distortion on LSR. To elucidate the differences resulting from the atomic scale fluctuations in composition and configuration, characteristic of MPEAs, we also calculate the Peierls stress in suitable reference materials, each of which contains one atomic type and hence bears no chemical compositional fluctuation. Three pure metals are considered as references — two are natural, Mo and Nb, and the third one is synthetic, a pure metal comprised of atoms with the average properties of MoNbTi, enabled by an *A*-atom potential. Ti is not considered as a reference metal because it has a hexagonal-close packed structure at ambient conditions. Due to their dissimilar atomic core structures, the LSRs of both edge and screw dislocations are calculated. We show that for neither screw nor edge dislocations, is the LSR on the {110} plane the lowest in MoNbTi, in contrast to Mo and Nb. For edge dislocations, the slip on the {134} plane is the easiest but for the screw dislocations, it is, on average, the hardest. For screw dislocations the {112} glide plane is the most favored while for edge dislocations it is the least favored. For the same type of glide plane, the LSRs for edge dislocations in MoNbTi are one to two orders of magnitude larger than the Peierls stress in the *A*-atom potential-based material. To explain the remarkable strengthening, the present analysis points to a combined effect of the lattice distortion and compositional fluctuation that cannot be captured by considering each factor alone.

2. Methodologies

Random solid solution MPEAs are created for LSR calculations as special quasirandom structures (SQS) [40] using ATAT [41]. In each SQS, the *y* axis is normal to one of the four types of slip planes: {110}, {112}, {123}, and {134} planes (see Table 1). The four SQSs, denoted as SQS_{110}, SQS_{112}, SQS_{123}, and SQS_{134}, respectively, contain 12, 24, 28, and 26 distinct atomic planes along the *y* axis. To account for all atomic planes within the same SQS, a series of derivative SQSs are built. For example, for SQS_{134}, 26 $SQSs^{\dagger}_{134}$ are constructed by sequentially moving the top atomic planes in SQS_{134} to the bottom, so that the mid-slip-planes (between the 13th and 14th atomic planes) of these $SQSs^{\dagger}_{134}$ differ in local atomic environment. The same method is employed to build 12 $SQSs^{\dagger}_{110}$, 24 $SQSs^{\dagger}_{112}$, and 28 $SQSs^{\dagger}_{123}$.

Next, a set of 3D simulation cells is constructed by replicating each $SQS^{\dagger}$ along the *x* and *y* directions, respectively, as illustrated

Table 1
For an edge or a screw dislocation, four PAD models are constructed. Summarized here are the crystallographic orientations.

		{110}	{112}	{123}	{134}
Screw	*x*	$[\bar{1}\bar{1}2]$	$[\bar{1}10]$	$[\bar{5}41]$	$[\bar{5}7\bar{2}]$
	y	$[1\bar{1}0]$	$[\bar{1}\bar{1}2]$	$[\bar{1}\bar{2}3]$	$[\bar{3}\bar{1}4]$
	z	[111]	[111]	[111]	[111]
Edge	*x*	[111]	[111]	[111]	[111]
	y	$[1\bar{1}0]$	$[\bar{1}\bar{1}2]$	$[\bar{1}\bar{2}3]$	$[\bar{3}\bar{1}4]$
	z	$[11\bar{2}]$	$[1\bar{1}0]$	$[5\bar{4}\bar{1}]$	$[5\bar{7}2]$

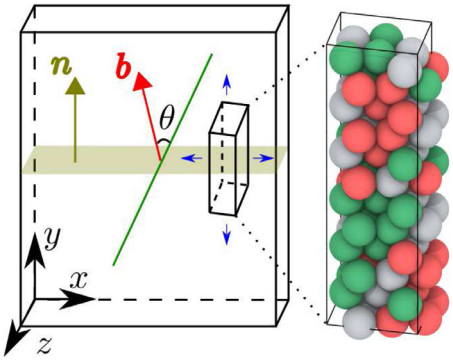

Fig. 1. Simulation box set-up for an edge ($\theta = 90^\circ$) or a screw ($\theta = 0^\circ$) dislocation. The dislocation line, Burgers vector, and slip plane are indicated by green line, red arrow, and a light-brown parallelogram, respectively. The simulation cell is built by repeating any SQS† (only SQS$^\dagger_{110}$ is shown here) along the x and y directions, as indicated by the blue arrows. Red, green, and grey atoms are, respectively, Mo, Nb, and Ti.

in Fig. 1. The crystallographic orientations of the three orthogonal directions of these cells for the four structures are summarized in Table 1. Periodic boundary conditions are applied on the x and z directions, while the y boundaries are traction-free. A single dislocation of edge or screw character is built into each cell by applying the corresponding isotropic elastic displacement fields to all atoms [42,43]. This configuration is known as the periodic array of dislocations (PAD) and was used in prior atomistic simulations to obtain Peierls stresses in BCC crystals, such as Fe [32,37,44] and Ta [45]. The center of the dislocation is situated at the mid-slip-plane in each cell [46,47]. As a result, even for the same type of slip plane (normal to the y axis), the local atomic environment around the dislocation core differs among the cells. For the three orthogonal edge lengths of the cell, L_x, L_y, and L_z, we set $L_x = 40$ nm, $L_y = 50$ nm, and $L_z \approx 1$ nm. In each cell, we assigned atoms within r_{mc} from the top and bottom y boundaries as "y-boundary layers", where $r_{\mathrm{mc}} = \max[r_c]$ is the maximum cutoff distance of the interatomic potentials among all elements.

To deform the simulation cells to move the dislocation, an incremental strain tensor $\Delta\boldsymbol{\epsilon}$ with one component being non-zero is applied to the simulation cell. For screw and edge dislocations, respectively, $|\Delta\epsilon_{yz}| = 10^{-6}$ and $|\Delta\epsilon_{yx}| = 10^{-5}$. The other eight components of $\Delta\boldsymbol{\epsilon}$ are set to zero. In each case, when the non-zero component is positive and negative, respectively, the dislocation is driven "forward" or along the positive x direction, and "backward" or along the negative x direction. For instance, for edge dislocations on the $(1\bar{1}0)$, $(\bar{1}\bar{1}2)$, $(\bar{1}\bar{2}3)$, and $(\bar{3}\bar{1}4)$ planes, the forward direction is [111] and the backward direction is $[\bar{1}\bar{1}\bar{1}]$. Note that prior MS simulations demonstrated that this simulation cell size is sufficiently large and the strain increment is sufficiently small to remove size effects on the Peierls stress of an edge dislocation on the {110} plane in Fe [32].

After each strain increment, the dislocated system is relaxed via the conjugate gradient scheme and the fast inertial relaxation engine [48]. During the energy minimization step, atoms in the y-boundary layers are allowed to relax only along two non-shear directions, which are x and y for the screw dislocation and y and z for the edge dislocation. The remaining atoms are free to relax along all three directions. The LSR σ_{L} is measured as the minimum virial stress of the system at which the dislocation moves at least 1 nm from its original position. The dislocation line is sufficiently short that all points on the lines move together and the line remains straight during glide and no kink-pair forms. The same procedure is followed to obtain the Peierls stresses σ_{P} for the reference metals, Mo, Nb, and the A-atom potential-based MoNbTi, the last of which will be denoted as MoNbTi$_A$ in what follows.

MS simulations are carried out using LAMMPS [49] and atomistic structures are visualized using OVITO [50]. Two recently validated embedded-atom method (EAM) interatomic potentials in MoNbTi [51] are used, including an alloy potential and an A-atom potential. The alloy potential represents an MPEA with varying elements from one BCC lattice site to another. The A-atom potential, on the other hand, is used to create a synthetic pure metal MoNbTi$_A$, wherein all atoms are of the same type, with no chemical disorder or lattice distortion but retaining almost the same elastic moduli and lattice parameter as MoNbTi. In developing the alloy potential, the cutoff distances r_c for Mo, Nb, and Ti, respectively, are 3.86 Å, 4.04 Å, and 4.15 Å. Hence, $r_{\mathrm{mc}} = 4.15$ Å. For the A-atom potential, $r_c = 4.02$ Å, which is the arithmetic mean cutoff of the three constituent metals. The lattice parameter a_0 for MoNbTi from the alloy and A-atom materials is 3.234 Å. In comparison, the constituent EAM potentials for Mo [52] and Nb [53] produce $a_0 = 3.135$ Å and 3.3 Å, respectively. In all cases, the magnitude of the Burgers vector of a dislocation $b = \sqrt{3}a_0/2$.

As discussed in Sec. 1, a long dislocation in an MPEA usually attains a wavy configuration, suggesting that the slip resistance spatially varies along the line. A part or parts of the dislocation line bows out, and therefore, the slip resistance is a combination of line tension and LSR. Further, the wavy dislocation segment loses its original screw/edge character as a result of glide. The LSR, as defined, pertains to dislocations of characteristic length, rather than dislocations of arbitrarily long lengths. The dislocation of approximately one periodic length remains straight as it glides, preserving its dislocation character. Since there is no bow out, we can separate the local resistance from local effects of line tension. Further, long screw segments move by kink pairs, which are comprised of short screw and edge segments. Hence, the LSRs for screw and edge dislocations can shed light on the variable motion of kink pairs in an MPEA. Later, in Sec. 4.3, we remark on the implications of these findings on dislocation dynamics in MoNbTi, as well as other BCC MPEAs.

3. Results

3.1. Peierls stresses in Mo, Nb, and MoNbTi$_A$

To first establish reference values, we calculate the Peierls stresses σ_{P} for edge and screw dislocations in pure reference materials, Mo, Nb, and MoNbTi$_A$, on all four slip planes: {110}, {112}, {123}, and {134}, and for both forward and backward senses in the slip direction $\langle 111 \rangle$.

The Peierls stresses for edge dislocations are calculable in all cases and their values are presented in Table 2. Three interesting findings arise. First, for the same type of slip plane, the Peierls stress in MoNbTi$_A$ is significantly lower than those in Mo and Nb. For the {110} and {112} planes, σ_{P} in MoNbTi$_A$ are approximately half those in Nb and an order of magnitude lower than those in Mo. For the {123} and {134} planes, σ_{P} in MoNbTi$_A$ are an order of magnitude lower than those in Nb and two orders of magnitude lower than those in Mo. Second, for each type of slip plane, all three metals exhibit the same rank order in σ_{P}, wherein σ_{P} is the highest on the {112} plane and the lowest on the {110} plane. For the two higher order planes, {123} and {134}, σ_{P} lie in between and are nearly equal in value in both Nb and MoNbTi$_A$ (but not in Mo). Last, all types of slip planes, except the {110} plane, exhibit glide-direction asymmetry. The asymmetry ratios in σ_{P} range between 1 and 2. For the {112} planes, in particular, the forward and backward directions are known as the "twinning" (T) and "anti-twinning" (AT) directions, respectively [9]. In Fe, for instance, prior MS simulations reported an AT/T ratio in the Peierls stress of about

Table 2
Means ($\bar{\sigma}_L$) and standard deviations (s_L) of the LSR (in MPa) of dislocations in MoNbTi on four types of slip planes along both forward and backward directions. The minimum σ_L^{min} and maximum LSR σ_L^{max} for each type of dislocation on the same type of slip plane in MoNbTi are also presented. On the {112} planes, the two directions are also known as twinning (T) and anti-twinning (AT) directions, respectively. Peierls stresses (σ_P) of the same type of dislocations in Mo, Nb, and *A*-atom potential-based MoNbTi (subscript *A*) are shown as references. Cases in which the screw dislocation gliding is unstable are presented as "-".

Plane	Dislocation	Direction	Mo	Nb	MoNbTi$_A$	MoNbTi				
			σ_P	σ_P	σ_P	$\bar{\sigma}_L$	s_L	$s_L/\bar{\sigma}_L$	σ_L^{min}	σ_L^{max}
{110}	Screw	forward	-	-	-	1738	132	0.08	1425	1831
	Screw	backward	-	-	-	1419	295	0.21	1058	1979
	Edge	forward	50	6	3	353	209	0.59	21	863
	Edge	backward	50	6	3	326	180	0.55	85	613
{112}	Screw	forward (T)	2496	859	763	972	414	0.43	337	1728
	Screw	backward (AT)	3842	-	1170	1525	927	0.61	8	3622
	Edge	forward (T)	533	118	49	998	591	0.59	17	2080
	Edge	backward (AT)	734	99	46	793	352	0.44	161	1426
{123}	Screw	forward	-	-	-	1532	244	0.16	837	1755
	Screw	backward	-	-	-	1979	3	0.002	1975	1983
	Edge	forward	160	12	2	226	234	1.04	6	902
	Edge	backward	117	13	1	292	316	1.08	12	1017
{134}	Screw	forward	-	-	-	1791	410	0.23	1512	2655
	Screw	backward	-	-	-	2947	490	0.17	2712	3878
	Edge	forward	111	13	1	242	223	0.92	39	833
	Edge	backward	69	12	2	157	110	0.7	40	558

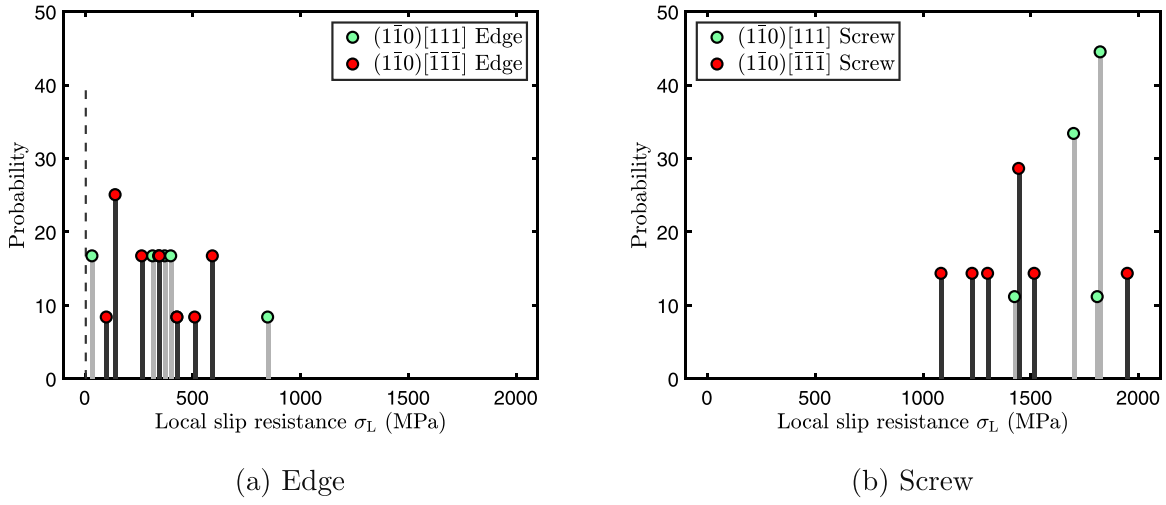

Fig. 2. Values of LSR σ_L associated with (a) edge and (b) screw dislocations on the {110} planes in MoNbTi. The vertical dashed line in (a) indicates the Peierls stress of an edge dislocation in MoNbTi$_A$.

1.1 for an edge dislocation on the {112} plane [10]. Here, the ratios are 1.38, 0.84, and 0.94 in Mo, Nb, and MoNbTi$_A$, respectively.

For screw dislocations, however, the Peierls stresses are incalculable in most cases. For the {110}, {123}, and {134} planes, when a shear strain is applied, along either the forward or the backward direction, the screw dislocation cross slips onto the {112} plane. In addition, when the strain is applied on the {112} plane in the backward direction, the screw dislocation in Nb (but not in Mo or MoNbTi$_A$) cross slips onto a non-parallel {112} plane. As a result, the Peierls stresses for screw dislocations are only calculable for the {112} planes in Mo and MoNbTi$_A$ in both directions and in Nb in the forward direction. Table 2 summarizes all Peierls stresses, where we designate the unstable gliding cases with "-".

The instabilities in screw dislocation glide are discussed in Appendix A and are attributed to the incorrect screw dislocation core structures. Here, the EAM potentials used for Mo [52] and Nb [53] were selected since they constitute the alloy potential for MoNbTi. As such, the Peierls stresses of pure metals are used solely as a basis for comparison with LSRs of MoNbTi. The goal is not to offer precise values for the Peierls stresses in Mo and Nb, which would be better obtained via machine learning-based interatomic potentials [14,54] or density functional theory (DFT). In particular, DFT has been applied to these two natural pure metals but mostly for the {110} screw dislocation, with the Peierls stress in Mo being 1350 MPa [55], 1600 MPa [56], 1800 MPa [57], 2420 MPa [89], or 2085 MPa [12], and that in Nb being 740 MPa [56].

To summarize, among the calculable Peierls stresses, MoNbTi$_A$ has lower σ_P compared to the constituent metals Mo and Nb for the same type of dislocation and slip plane. However, as will be shown next, the actual alloy, MoNbTi, with its characteristic compositional fluctuations, exhibits properties diametrically different from MoNbTi$_A$.

3.2. Local slip resistances in MoNbTi

Fig. 2 presents distributions of σ_L for edge and screw dislocations on {110} planes in MoNbTi. For both edge and screw dislocations, the values of σ_L vary substantially, over a large range of 842 MPa. For comparison, the Peierls stress for the edge dislocation in MoNbTi$_A$ is marked by a vertical dashed line. For the screw dislocations, 16 out of 24 local chemical environments lead to calculable LSR values, indicating that chemical deviations from the pure metal help stabilize glide. The statistical dispersion in LSRs arises directly from the differences in the chemical composition and lat-

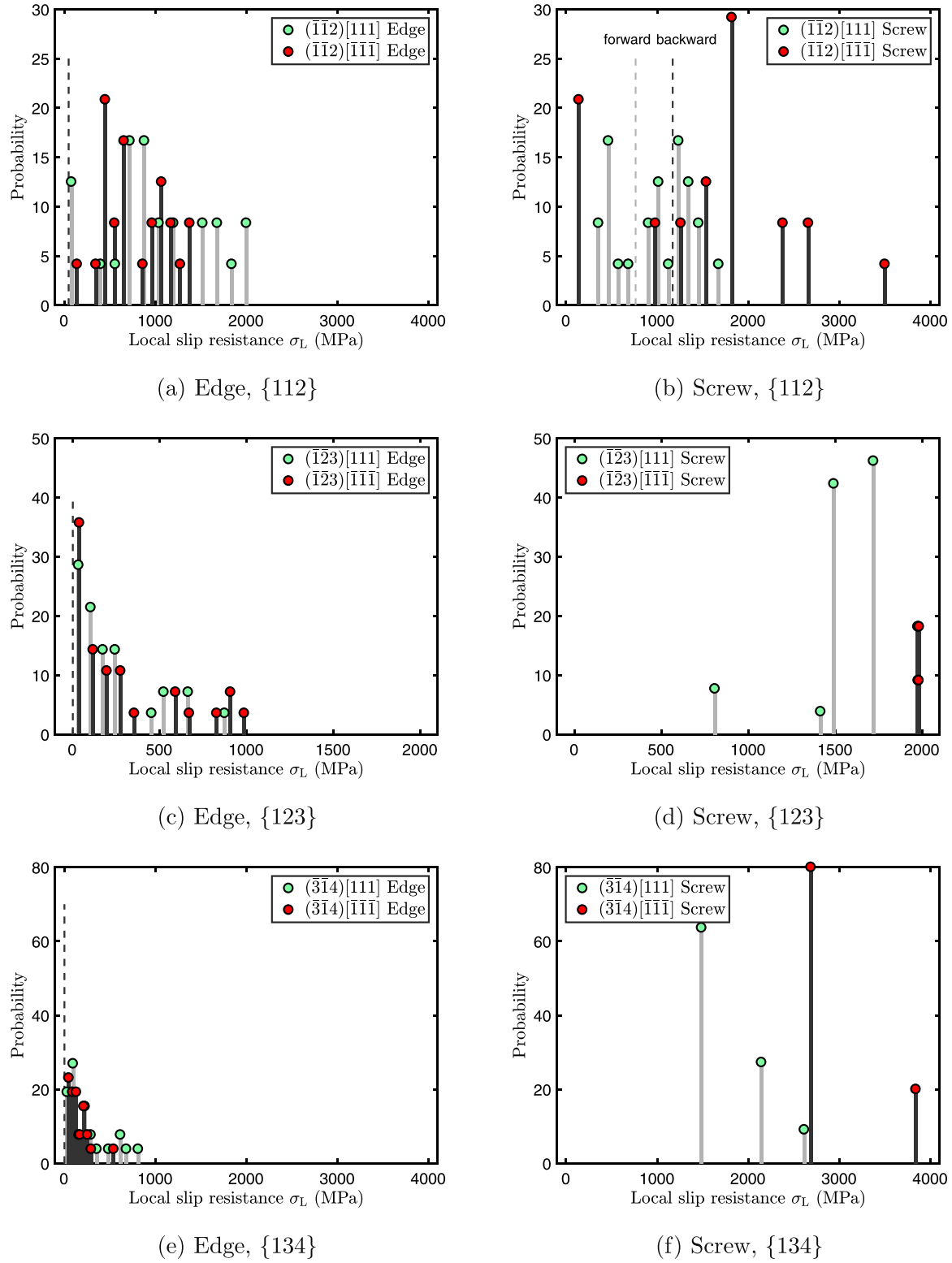

(a) Edge, {112} (b) Screw, {112}

(c) Edge, {123} (d) Screw, {123}

(e) Edge, {134} (f) Screw, {134}

Fig. 3. Values of LSR σ_L associated with (a,c,e) edge and (b,d,f) screw dislocations on the {112}, {123}, and {134} planes in MoNbTi. The vertical dashed lines indicate the corresponding Peierls stresses in MoNbTi$_A$.

tice distortion from one location to the next around the dislocation core and over the motion path taken by the dislocation. As a result, LSR is not equal in the forward and backward direction for the same plane. On average, the ratios in σ_L between the forward and backward directions are 1.22 and 1.08, for screw and edge dislocations, respectively. Similar local environment-induced asymmetry ratios, 0.89–1.02, were reported in prior MD work of an edge dislocation gliding on the {111} planes in equal-molar FCC NiFe under different applied stresses and at different temperatures [58]. Like the {110} planes in pure BCC metals, no glide-direction asymmetry is expected for the {111} planes in pure FCC metals.

Fig. 3 presents the σ_L distributions of edge and screw dislocations on the three higher order planes in MoNbTi. As for the {110} planes, these distributions exhibit outstanding statistical dis-

persion, with the coefficient of variations (COVs), i.e., ratio of the standard deviation to mean, over unity in some cases. For the edge dislocations, the COV ranges from 0.44 to 1.08, with the largest value associated with the backward direction on the {123} plane. In this particular case, the minimum and maximum LSR values, respectively, are 12 MPa and 1017 MPa, respectively, as presented in Table 2. For the screw dislocations, the COVs are between 0.002 and 0.61. Similar to the {110} planes, the glide of screw dislocations on the two highest order slip planes, {123} and {134}, can be stabilized. Out of the 56 and 52 total cases in {123} and {134} slip planes, respectively, glide of a screw dislocation was stable in 37 and 21 cases.

The LSR values exhibit a twinning/anti-twinning asymmetry on the {112} plane. On average, the ratios of σ_{L} for the anti-twinning direction to the twinning direction are 1.57 (screw) and 0.74 (edge), which are similar to those in MoNbTi$_A$, which are 1.53 (screw) and 0.94 (edge). Different from MoNbTi$_A$, the asymmetry ratio for the screw dislocation on a specific {112} plane in MoNbTi can be less than unity. Out of the total 24 distinct {112} planes, the twinning σ_{L} is higher than its anti-twinning counterpart for seven screw dislocations. This is uncharacteristic of BCC pure metals, in which the Peierls stress of a screw dislocation is always lower along the twinning direction than the opposite direction. Evidently, the effects of compositional variation and lattice distortion on LSR can be sufficiently strong to reverse the intrinsic twinning/anti-twinning asymmetry. Similarly, for edge dislocations on the {123} planes, while the mean value of σ_{L} is lower for the forward direction than for the backward direction, the asymmetry is reversed for some given planes. Specifically, on 11 out of the 28 {123} planes is σ_{L} higher for the forward direction than for the backward direction.

3.3. Anisotropy in the slip resistance

Studies of the LSR distributions on different types of slip planes provide insight into the preferred glide systems used by dislocations in deformed MoNbTi. Comparing the full distributions of edge dislocations indicate a preference for easy glide on the {123} and {134} planes, where most LSR values are less than 1000 MPa. Considering only the mean LSR values for the edge dislocation in Table 2, we observe their rank order from hardest to easiest to be $\bar{\sigma}_{\mathrm{L}}^{112} > \bar{\sigma}_{\mathrm{L}}^{110} > \bar{\sigma}_{\mathrm{L}}^{123} > \bar{\sigma}_{\mathrm{L}}^{134}$. In contrast, comparing the full LSR distributions of screw dislocations identifies a preference for glide on the {112} planes. The mean LSRs for screw dislocations follow the reversed rank order from that for edge dislocations, i.e., $\bar{\sigma}_{\mathrm{L}}^{134} > \bar{\sigma}_{\mathrm{L}}^{123} > \bar{\sigma}_{\mathrm{L}}^{110} > \bar{\sigma}_{\mathrm{L}}^{112}$. The slip resistance rank order seen in the edge and screw dislocation LSRs are not the same as that in the Peierls stresses of edge dislocations in Mo, Nb, and MoNbTi$_A$, which is: $\sigma_{\mathrm{P}}^{112} > \sigma_{\mathrm{P}}^{123} > \sigma_{\mathrm{P}}^{134} > \sigma_{\mathrm{P}}^{110}$. It is commonly found that the Peierls stress on the {110} plane is the easiest in Nb [59,60] and other BCC metals [16], and is one reason it is the most studied glide plane to date [61].

As a measure for anisotropy in slip resistance, we consider the COV among mean LSR values of all four slip planes in both the forward and backward directions. This calculation entails the COV for a set of eight mean LSR values, i.e.,

$$\mathrm{COV} = \frac{\text{Standard deviation of } \{\bar{\sigma}_{\mathrm{L}}^{s}\}}{\text{Mean of } \{\bar{\sigma}_{\mathrm{L}}^{s}\}} \tag{1}$$

or for a pure metal, the analogous anisotropy indicator is the COV for a set of eight Peierls stress values, i.e.,

$$\mathrm{COV} = \frac{\text{Standard deviation of } \{\sigma_{\mathrm{P}}^{s}\}}{\text{Mean of } \{\sigma_{\mathrm{P}}^{s}\}} \tag{2}$$

where $s = 1, 2, \ldots, 8$ is a slip mode associated with a specific slip plane and a specific direction. In MoNbTi, the results are 0.33 and 0.71 for the screw and edge dislocations, respectively. In contrast, for the Peierls stresses of the edge dislocations in pure metals, the corresponding COVs are 1.13, 1.31, and 1.58 in Mo, Nb, and MoNbTi$_A$, respectively. Evidently, the anisotropy in slip resistance is greatly reduced in the MPEA compared with in pure metals.

Table 3
The ratios in the mean LSR ($\bar{\sigma}_{\mathrm{L}}$) between the screw and edge dislocations in MoNbTi are presented, based on the data in Table 2. The same ratios in the Peierls stresses (σ_{P}) in Mo, Nb, and *A*-atom potential-based MoNbTi (subscript *A*) are shown as references. Cases in which the screw dislocation gliding is unstable are presented as "-".

Plane	Direction	Mo	Nb	MoNbTi$_A$	MoNbTi
{110}	forward/backward	-	-	-	4.65
{112}	forward	4.68	7.28	15.57	0.97
{112}	backward	5.23	-	25.43	1.92
{123}	forward	-	-	-	6.78
{123}	backward	-	-	-	6.78
{134}	forward	-	-	-	7.4
{134}	backward	-	-	-	18.77

Another measure of the slip resistance anisotropy is the ratio $\bar{\sigma}_{\mathrm{L}}^{112}/\bar{\sigma}_{\mathrm{L}}^{110}$, since, as seen here and other work, in pure metals, Peierls stresses on these planes mark two extremes. Here, for the edge dislocations, $\sigma_{\mathrm{P}}^{112}/\sigma_{\mathrm{P}}^{110}$ in Mo, Nb, and MoNbTi$_A$ range from 10.66 to 19.67. For the edge dislocations in MoNbTi, the ratios $\bar{\sigma}_{\mathrm{L}}^{112}/\bar{\sigma}_{\mathrm{L}}^{110}$ are much smaller — 2.25 for the forward direction and 3.06 for the backward direction. For screw dislocations, the ratios are even smaller: 0.56 and 1.07 for the forward and backward directions, respectively.

Our calculations also point to reduced screw-to-edge ratios in the slip resistance in the MPEA than in pure metals. These ratios can serve as input parameters to continuum models, e.g., the phase-field dislocation model (PFDM) [62]. Table 3 presents these ratios in all four materials. In pure metals, the ratios $\sigma_{\mathrm{P}}^{\mathrm{screw}}/\sigma_{\mathrm{P}}^{\mathrm{edge}}$ are only available for the {112} plane due to the instabilities in screw dislocation gliding on other planes. For the {112} plane in MoNbTi, the ratio $\bar{\sigma}_{\mathrm{L}}^{\mathrm{screw}}/\bar{\sigma}_{\mathrm{L}}^{\mathrm{edge}}$ is strikingly low, ranging from 0.97 to 1.92, much lower than those in the {112} Peierls stresses in any of the pure metals. In MoNbTi, the {123} and {134} planes have the largest screw-to-edge LSR ratio, ranging from 6.78 to 18.77. Yet still, these are lower than that in the Peierls stress along the backward direction on the {112} plane in MoNbTi$_A$, for which the ratio is 25.43. Low $\bar{\sigma}_{\mathrm{L}}^{\mathrm{screw}}/\bar{\sigma}_{\mathrm{L}}^{\mathrm{edge}}$ ratios on the {110} planes have been reported previously in several BCC MPEAs, including $NbTi_2Zr$, for which the ratio measured in experiments is 6.3 [20]; NbTiZr, for which the ratio from MD simulations is 2 [21]; $Co_{16.67}Fe_{36.67}Ni_{16.67}Ti_{30}$, for which the ratio is 1.1–1.2, as estimated by MD simulations [22]; and MoNbTaW, for which the ratio is 2.73 based on MD calculations [14]. To the best of our knowledge, screw-to-edge ratios for dislocations in BCC MPEAs outside of the {110} planes have not been reported in the literature.

4. Discussion

4.1. Correlation of LSR values with ideal shear strengths

Another common property used for identifying preferred slip modes is the ideal shear strength, T_{is}, for the glide plane. The more likely glide planes tend to possess a lower T_{is}, which is defined as the maximum value of the ideal shear stress, τ_{is}, which is the gradient of the generalized stacking fault energy (GSFE) curve [63], i.e.,

$$\tau_{\mathrm{is}}(d_0) = \frac{\partial \gamma_{\mathrm{gsf}}(d_0)}{\partial d_0} \tag{3}$$

$$T_{\mathrm{is}} = \max\left[\tau_{\mathrm{is}}(d_0)\right] \tag{4}$$

Table 4
Means ($\bar{T}_{is}$) and standard deviations (s_{is}) of the ideal shear strength (in GPa) in MoNbTi on the four slip planes. Ideal shear strengths (T_{is}) in Mo, Nb, and *A*-atom potential-based MoNbTi (subscript *A*) are shown as references.

Plane	Mo	Nb	$MoNbTi_A$	MoNbTi		
	T_{is}	T_{is}	T_{is}	$\bar{T}_{is}$	s_{is}	$s_{is}/\bar{T}_{is}$
{110}	33.1	14.1	14.8	15.2	2.1	0.14
{112}	58.4	24.5	25.8	27.5	3.8	0.14
{123}	19.3	8.1	8.5	8.7	1.2	0.14
{134}	18.9	7.9	8.4	8.5	0.8	0.09

where the rigid shift along the ⟨111⟩ direction, d_0, is in units of b and ranges from 0 to 1.

Like LSR values, the GSFE curves depend on the local chemical composition in the plane and, thus, vary substantially among parallel slip planes for the same type of plane in the same MPEA [64]. Applying Eqs. (3) and (4) to the GSFE curves of MoNbTi from Ref. [51], the distributions of T_{is} for each slip plane type can be calculated and their means and standard deviations are presented in Table 4. For comparison, T_{is} for the natural references, Mo and Nb, and the synthetic one, $MoNbTi_A$ are also calculated from their respective GSFE curves, which are also from Ref. [51]. As expected, T_{is}, representing the strength of a dislocation-free crystal, are two to four orders of magnitude larger than the LSRs and Peierls stresses, which are associated with the strength of a dislocated crystal.

Interestingly, the slip plane rank order based on T_{is} is the same for MoNbTi and the three references, with {123} and {134} being the easiest glide planes and {112} being the hardest one. This rank order is the same as that in the edge LSR, but not the screw LSR, in MoNbTi. The concurrence can be expected since the in-plane ideal shearing, which is along the ⟨111⟩ direction, better represents the motion of edge dislocations, which is along ⟨111⟩, than that of screw dislocations, which is along a non-⟨111⟩ direction within the slip plane which, in our case, is the x axis (Table 1).

The GSFE curves and the derived values of T_{is} reflect only the compositional fluctuations on bond strengths across the plane of shear. The two orders of magnitude differences between the LSRs in MoNbTi and the Peierls stresses in $MoNbTi_A$ are not reflected in T_{is}. For the same type of slip plane, the values of T_{is} in $MoNbTi_A$ are almost the same as the mean values $\bar{T}_{is}$ in MoNbTi. In addition, T_{is} in $MoNbTi_A$ are noticeably close to those in Nb, in contrast to that $MoNbTi_A$ has much lower Peierls stresses than Nb. The failure of T_{is} to replicate the profound strengthening seen in the LSR for the MPEA over the pure metals suggests that the properties not reflected in the GSFE calculation, e.g., the lattice distortion within a small atomic environment, are the reason why MPEAs are strong.

While T_{is} is not a good reflection of the strengthening effects in dislocation glide resistance, it is possible that T_{is} at least scales in the same way as the LSR. Fig. 4 compares the distributions of the normalized LSR for edge and screw dislocations with those for the normalized T_{is}. Despite the significant statistical variations, LSRs are reasonably correlated with T_{is}, with higher LSRs signifying higher T_{is} and vice versa. This suggests that the LSR values can evidently give some insight into the slip plane preferences for dislocations.

4.2. Strengthening in MoNbTi

Direct comparison of σ_L in MoNbTi with σ_P in $MoNbTi_A$ indicates that the former is the stronger material. For edge dislocations, the mean LSR value in MoNbTi is substantially larger, by one to two orders of magnitude, than the Peierls stress in $MoNbTi_A$, for every plane type. Compared to the natural pure metals, Mo and Nb, the LSR values for the edge dislocations in MoNbTi are higher than their Peierls stresses, but not as outstanding as when compared to $MoNbTi_A$. For screw dislocations, the same comparison can only be carried out for the {112} planes. The mean values of σ_L in MoNbTi are only 27% higher in the twinning direction and 30% higher in the anti-twinning direction than respective σ_P in $MoNbTi_A$. In addition, the mean LSR for the screw dislocations in MoNbTi are higher than the Peierls stresses for the same type of dislocations in Nb, but much lower than those in Mo. In other words, the strengthening effect in MoNbTi is profound for edge dislocations, and less so for screw dislocations. Together they result in small screw-to-edge ratios in the slip resistance in MoNbTi.

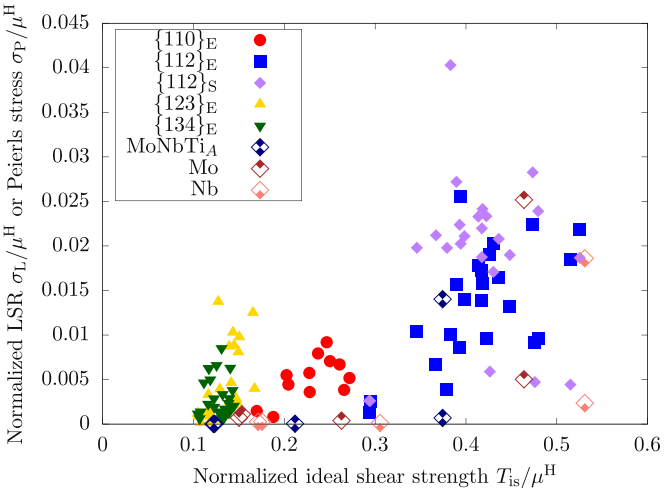

Fig. 4. Normalized LSR σ_L/μ^H and normalized Peierls stress σ_P/μ^H are plotted with respect to normalized ideal shear strength T_{is}/μ^H for the same specific plane in MoNbTi, *A*-atom potential-based MoNbTi (subscript *A*), Mo, and Nb. μ^H is the isotropic shear modulus in Hill form. Values of μ^H in the four materials were provided in Ref. [51]. E and S stand for edge and screw dislocations, respectively. For each specific plane, values of σ_L and σ_P for the same type of dislocation are averaged over two opposite directions. For MoNbTi, five sets of dislocations/slip planes are distinguished by different filled symbols and colors. For each of $MoNbTi_A$, Mo, and Nb, the same partly filled symbol and color are used for all five sets of dislocations/slip planes.

In MPEAs, two characteristics are important — the chemical compositional fluctuation and lattice distortion. Many prior studies have measured nominal or bulk average values of these quantities and found meaningful correlations between them and material properties. For instance, higher degrees of chemical short-range order in FCC CoCrNi were found to lower the average velocity of the Shockley partial dislocations [65]. Combined experimental and theoretical work on ten FCC Ni-based binaries and MPEAs [66] and nine BCC Nb-based binaries and MPEAs [67] have demonstrated that larger lattice distortion were reasonably correlated with higher lattice friction stresses. In those work, each MPEA possessed one average value for chemical ordering, dislocation velocity, lattice distortion, and lattice friction stress.

In this work, we study the distribution of the *local* slip resistance, i.e., LSR, among dislocations that sit in different *local* regions in the same MPEA, MoNbTi. The variations in LSR point to the significance of the local atomic environment on the motion of an elementary dislocation segment. To identify possible causes of the variation, we consider the local chemical composition and local lattice distortion (LLD) in every local environment in MoNbTi and seek, if any, correlation between them and the corresponding LSR. All calculations are performed on atoms in a region within a distance of $\pm b/2$ from the slip plane along the y axis. Because the inter-slip-planar spacing depends on the crystallography, the small volumes (≈ 5–$10b^3$) span 2, 4, 6, and 6 layers of atoms for

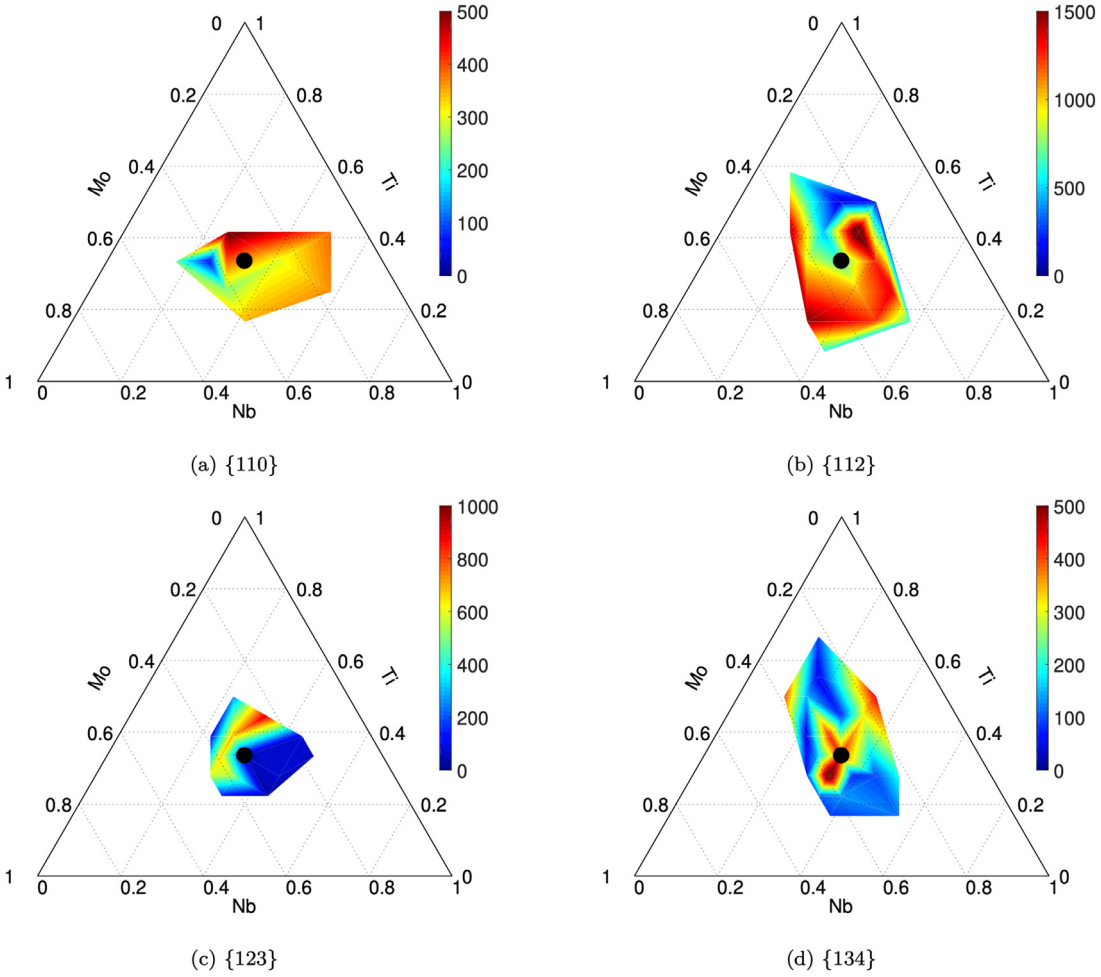

Fig. 5. LSR values (in MPa) of the edge dislocation averaged over two opposite directions on the same specific plane correlated with the local chemical compositions in MoNbTi. The black circles in the center indicate the equal-molar composition. Results are based on the alloy potential.

the {110}, {112}, {123}, and {134} planes, respectively. The selected characteristic length is reasonable because (i) the dislocation cores in a series of FCC MPEAs were found to extend to about b–1.5b [68] and (ii) dislocation cores are usually smaller in BCC metals than in FCC metals [69].

In Fig. 5, LSRs for edge dislocations are mapped onto a ternary composition diagram. As shown, the range of compositions sampled in the LSR calculations deviates substantially from the equal-molar one. The relative ratios of certain elements do not have consistent effects across planes. For the {112} planes, the highest LSR value corresponds to compositions with a large proportion of Mo. For the {110} and {123} planes, however, larger fractions of Mo tend to reduce LSR.

Evidently, the compositional deviations from one dislocation environment to the next contribute to the variation in LSR, yet they only play a part in determining the level of statistical variation in LSR. For instance, while the composition range for the {123} planes is the smallest, its COV in LSR of dislocations is the largest, being over unity. By interpolation we can locate the value of σ_{L} associated with the equal-molar composition: 355 MPa for the {110} plane, 865 MPa for the {112} plane, 34 MPa for the {123} plane, and 418 MPa for the {134} plane. Even with nearly the same composition, the LSR values are still one to two orders of magnitude higher than the corresponding Peierls stresses in MoNbTi$_A$. This substantial difference confirms that it is the structural distortions and variable chemical bonding particular to the atomic neighborhood surrounding the dislocation core that give rise to the profound strengthening seen in the MPEA over a pure metal.

Lattice distortion can be calculated at the bulk scale [70] for the entire MPEA or at the local scale [71] for an atomic-sized characteristic volume. The latter is LLD and can be calculated following Ref. [72], via

$$\beta_{\mathrm{L}} = \frac{1}{Na_{\mathrm{N}}} \sum_i \sqrt{(x_i - x_i')^2 + (y_i - y_i')^2 + (z_i - z_i')^2} \tag{5}$$

where N is the number of atoms within the local region, a_{N} is the first nearest neighbor distance, (x_i, y_i, z_i) and (x_i', y_i', z_i') are the coordinates of unrelaxed and relaxed positions of atom i, respectively. Since the underlying lattice in MoNbTi is BCC, $a_{\mathrm{N}} = b$.

Fig. 6 maps on a ternary diagram the LLD for the small volumes defining the LSR for edge dislocations for each type of slip plane. The LLD in each is expected to vary with chemical composition, since it is the direct result of the different types of atoms occupying the lattice sites within these volumes. The LLD is also affected by the inter-slip-planar spacing, nominally increasing with decreasing spacing from {110} to {134}. In accordance, we observe that the range of LLD for the {110} and {112} planes is lower than that for the {123} and {134} planes. By interpolation, the values of LLD associated with the equal-molar composition are 0.0989 for the {110} plane, 0.1043 for the {112} plane, 0.1166 for the {123} plane, and 0.1263 for the {134} plane. In all cases, the composition yielding the highest and lowest LLD lies outside the equimolar composition. Using Eq. (5), we also calculate the bulk lattice distor-

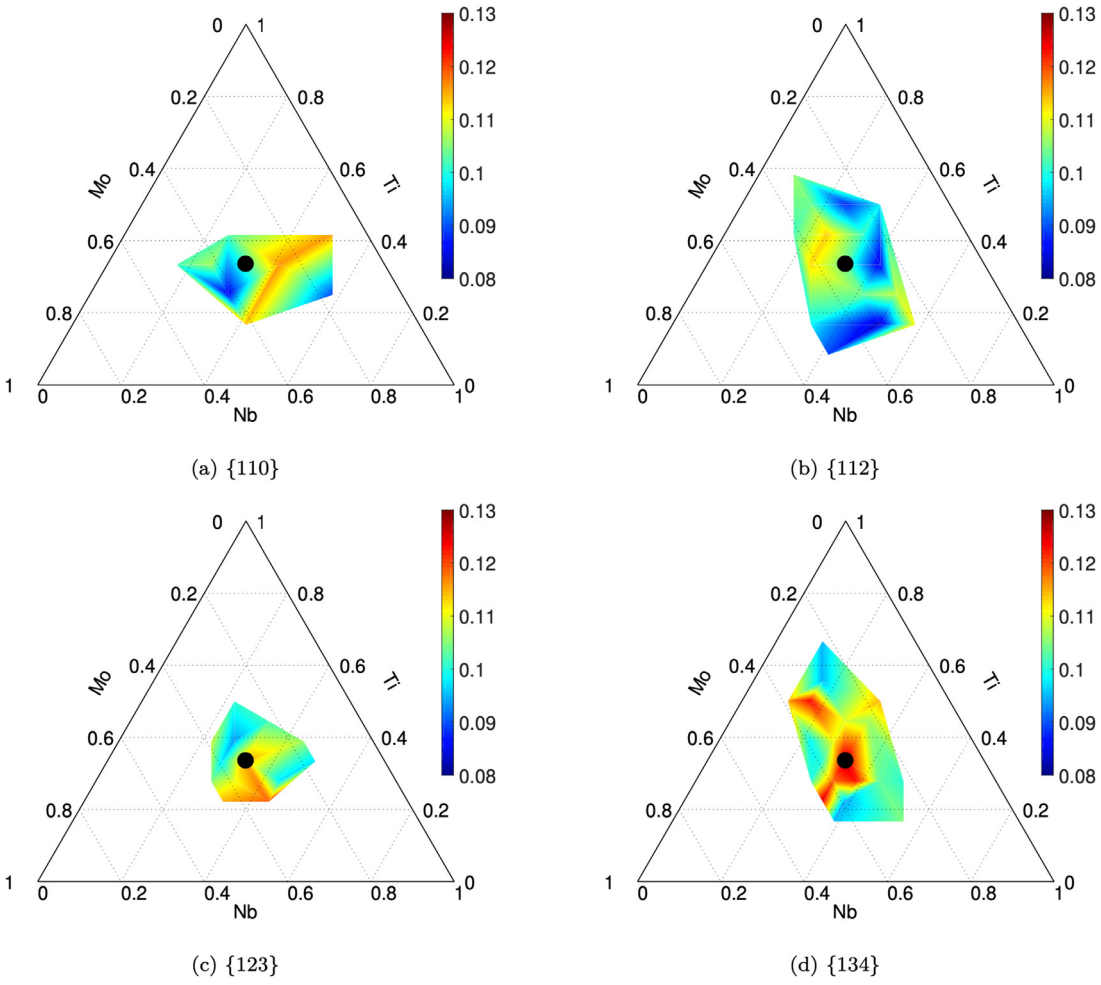

(a) {110} (b) {112}

(c) {123} (d) {134}

Fig. 6. LLD values for the edge dislocation cases correlated with the local chemical compositions in MoNbTi. The black circles in the center indicate the equal-molar composition. Results are based on the alloy potential.

tion in the four simulation cells of random equimolar MoNbTi. The average lattice distortion is 0.106 ± 0.003, close to that of the LLD for the {112} plane for the equimolar composition.

The analysis shows that both local chemical composition and LLD vary substantially from one characteristic small volume to the next among different glide planes, even within the same MPEA. Comparing the LSR maps in Fig. 5 with the LLD maps in Fig. 6 indicates that on the {110} plane more Ti and/or Nb atoms in the local environment tend to result in both high LLD and high LSR. For the {134} plane, the equimolar composition or close to it produces both high LSR and high LLD. Yet at the same time, for the same type of slip plane, some compositions yielding the relatively higher LLD do not necessarily lead to the higher LSR. Note that both LLD and LSR values are affected by the arrangement of the atoms, which is not reflected in the ternary map. Two volumes with the same composition can bear different arrangements, hence lattice distortion, and consequently LSRs.

4.3. Implications for dislocation dynamics in MoNbTi and other BCC MPEAs

While we only evaluate the slip resistances of short dislocation segments that remain straight during glide, the results can provide insight into actual slip propensities of long dislocations in MoNbTi. Compared with pure metals, two key features found here for MoNbTi are: (i) a wide range of slip resistances even for the same type of dislocation and slip plane, and (ii) the significantly reduced anisotropy in the slip resistance. The first finding is directly related to the wavy configuration of long dislocations in MoNbTi observed in a recent transmission electron microscopy (TEM) study [25], because the slip resistance varies spatially along the same line. Atomistic simulations [21,22,28], discrete dislocation dynamics [73], and PFDM [62] of the glide of long screw and edge character dislocations in BCC MPEAs have reported wavy dislocation morphologies resulting from continuous pinning and depinning at points encountered within the slip plane during active glide. The results are not limited to glide in BCC metals. Recent atomistic simulations [74,75], PFDM [76], and *in situ* TEM studies [77] of the glide of long dislocations in FCC MPEAs have reported wavy motion, indicating that some local atomic neighborhoods are harder for the dislocation to bypass than others. Particularly for screw dislocations, it also suggests that cross slip is promoted because a screw dislocation may switch from a relatively resistant slip plane to a non-parallel, less resistant one [78]. For example, in FCC solid solution alloys, while on average the energy barrier for cross slip is higher than that in pure metals, some segments along the dislocation line can have a very low barrier and hence cross slips easily [79]. This reduces the cross slip energy barrier for the remaining dislocation segments, and consequently, the entire dislocation line cross slips more easily compared with FCC pure metals [80]. Massive dislocation cross slip was recently reported in FCC MPEAs in experiments [81] and MD simulations [82]. Indeed, in-

troducing randomness at the atomic scale brings new length and energy scales that affect dynamics of many defects (e.g., vacancies, dislocations, intrinsic stacking faults, grain boundaries, and cracks), resulting in novel alloy properties [83].

The second finding points to the increased significance of edge dislocations in plasticity of MoNbTi and a multiplicity of slip modes. The differences in the slip resistance anisotropy between MoNbTi and pure metals indicate that novel dislocation dynamics can occur in the former. For example, since dislocations in MoNbTi can easily glide on high order crystallographic planes, strong interactions among multiple slip systems are expected. The TEM study in MoNbTi mentioned above reported that the frequent planes on which dislocations glide are {112}, {123}, and {134}, on which the critical resolved shear stresses are, respectively, 455 MPa, 398 MPa, and 235 MPa [25]. Interestingly, little to no dislocations were found on the {110} plane. These are corroborated by the present LSR calculations in that neither edge nor screw dislocation favors the {110} plane. The same experiment also revealed that the dislocations gliding on higher order planes have a predominantly non-screw character, which is consistent with the reduced screw-to-edge ratio in slip resistance found in our simulations. Indeed, when non-screw dislocation glide governs plasticity, dislocations would be expected to predominantly glide on the two highest order planes, {123} and {134}, which possess the lowest LSR values for edge dislocations (Table 2). Note that the screw-to-edge ratios in slip resistance on these two types of planes are higher than those on the {112} plane in Mo and Nb (Table 3), implying that the dislocation motion in MoNbTi could occur via kink-pair motion, as in pure metals. This finding in MoNbTi also suggests that investigation of the slip resistances or more generally dislocation dynamics in other BCC MPEAs need to go beyond the most often studied {110} plane.

5. Conclusions

In this work, we conduct MS simulations to calculate the LSR in equal-molar refractory MoNbTi MPEA, which has a BCC lattice. TEM experiments on this MPEA provided evidence that dislocations can glide on higher order glide planes, {112}, {123}, and {134} planes [25]. Here, LSR is defined as the critical stress for a short dislocation line ($\leq$ 1 nm) to glide by at least 1 nm, while remaining straight and not moving by kink-pair formation. With dissimilar atomic core structures, both edge and screw dislocations are considered. To quantify effects of chemical fluctuation and lattice distortion on slip resistances, the Peierls stresses of the same type of dislocations in Mo, Nb, and *A*-atom potential-based MoNbTi$_A$ are also calculated. It is found that, due to the spatial variation in local chemical composition in MoNbTi, the LSR values vary significantly with the COVs ranging from 0.002 to 1.08 for the same dislocation on the same type of slip plane. The LSR values for the edge dislocations are, on average, two orders of magnitude higher than the Peierls stresses in MoNbTi$_A$, which possesses the same bulk properties as MoNbTi but with no lattice distortion or chemical compositional fluctuation. Edge dislocations in MoNbTi tend to glide on the two highest order planes {123} and {134} than the more often studied {110} and {112} glide planes in pure BCC metals. For screw dislocations, however, the mean LSRs are only 27–30% stronger than those in pure metals, leading to a substantially reduced screw-to-edge ratio in MoNbTi than in MoNbTi$_A$. In addition, the slip plane anisotropy in the LSR is much lower in MoNbTi than that in the Peierls stress in pure metals. The strengthening and lowering of screw-to-edge ratio in the LSR results from a synergistic effect involving both chemical compositional fluctuation and lattice distortion. All these are intimately related to the unusual dislocation dynamics and unique mechanical properties in BCC MPEAs.

Declaration of Competing Interest

The authors declare that they have no known competing financial interests or personal relationships that could have appeared to influence the work reported in this paper.

Acknowledgements

We thank Dr. Fulin Wang, Dr. Sheng Yin, Dr. Xiang-Guo Li, and Dr. Dengke Chen for helpful discussions. The work of SX was supported in part by the Elings Prize Fellowship in Science offered by the California NanoSystems Institute (CNSI) on the UC Santa Barbara campus. SX, YS, and IJB gratefully acknowledge support from the Office of Naval Research under contract ONR BRC Grant N00014-18-1-2392. Use was made of computational facilities purchased with funds from the National Science Foundation (CNS-1725797) and administered by the Center for Scientific Computing (CSC). The CSC is supported by the CNSI and the Materials Research Science and Engineering Center (MRSEC; NSF DMR 1720256) at UC Santa Barbara. This work used the Extreme Science and Engineering Discovery Environment (XSEDE), which is supported by National Science Foundation grant number ACI-1053575.

Appendix A. Instabilities in screw dislocation glide

As discussed in Sec. 3.1, the screw dislocation glide is unstable on {110}, {123}, and {134} planes in Mo, Nb, and MoNbTi$_A$, and also for the backward (i.e., anti-twinning) direction on the {112} plane in Nb. Analyses of the atomistic structures reveal that the

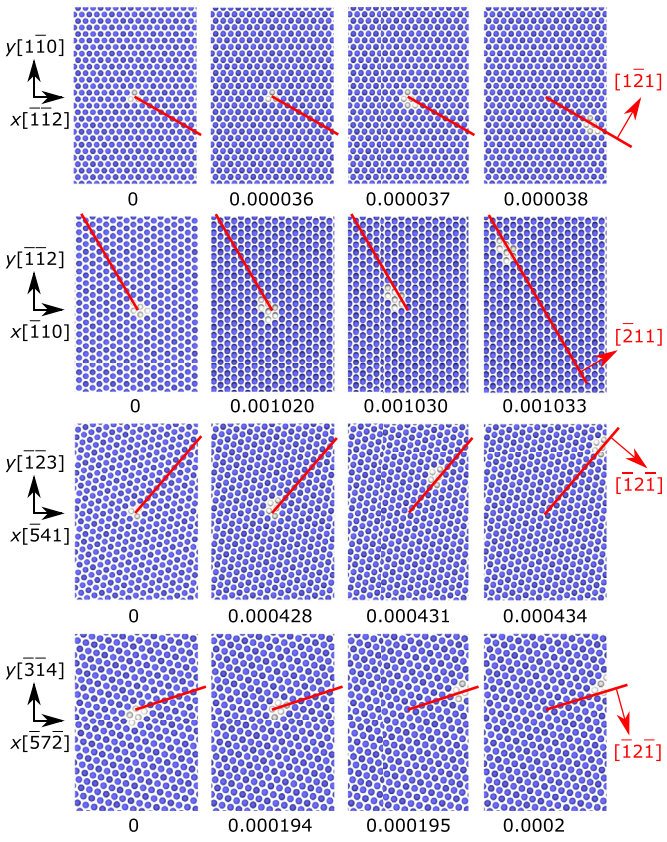

Fig. A.1. Unstable gliding of a screw dislocation at different strains in Nb. The first, second, third, and fourth row, respectively, corresponds to the {110}-forward, {112}-backward, {123}-forward, and {134}-forward case. In all snapshots, the *z*[111] axis is along the out-of-plane direction. Blue and white atoms are those in BCC and disordered local lattices, respectively. Red lines indicate {112} planes.

screw dislocation frequently cross slips onto non-parallel, alternating {110} planes, resulting in an effectively composite glide on the {112} plane, as shown in Fig. A.1. The instability of a screw dislocation gliding on an initially prescribed {110} plane has been reported in prior MS simulations in Nb [84] and Ta [13,85–87]. The same frequent cross slip was reported in those work and was attributed to the incorrect screw dislocation core structures calculated by those particular EAM potentials [87]. Some other EAM potentials, however, have been able to calculate the Peierls stress for screw dislocations on the {110} plane in some BCC metals. For example, EAM-based MS simulations in Fe [38,88] and Mo [86] revealed stable glide of a screw dislocation on the {110} plane, enabling calculation of those Peierls stresses.

References

[1] J.-W. Yeh, S.-K. Chen, S.-J. Lin, J.-Y. Gan, T.-S. Chin, T.-T. Shun, C.-H. Tsau, S.-Y. Chang, Nanostructured high-entropy alloys with multiple principal elements: Novel alloy design concepts and outcomes, Adv. Eng. Mater. 6 (5) (2004) 299–303, doi:10.1002/adem.200300567.

[2] B. Cantor, I.T.H. Chang, P. Knight, A.J.B. Vincent, Microstructural development in equiatomic multicomponent alloys, Mater. Sci. Eng. A 375-377 (2004) 213–218, doi:10.1016/j.msea.2003.10.257.

[3] E. Ma, Unusual dislocation behavior in high-entropy alloys, Scripta Mater. 181 (2020) 127–133, doi:10.1016/j.scriptamat.2020.02.021.

[4] R. Peierls, The size of a dislocation, Proc. Phys. Soc. 52 (1) (1940) 34, doi:10.1088/0959-5309/52/1/305.

[5] W.-R. Jian, M. Zhang, S. Xu, I.J. Beyerlein, Atomistic simulations of dynamics of an edge dislocation and its interaction with a void in copper: a comparative study, Modelling Simul. Mater. Sci. Eng. 28 (4) (2020) 045004, doi:10.1088/1361-651X/ab8358.

[6] P.M. Anderson, J.P. Hirth, J. Lothe, Theory of Dislocations, 3, Cambridge University Press, Cambridge, 2017.

[7] S. Xu, Modelling plastic deformation of nano/submicron-sized tungsten pillars under compression: A coarse-grained atomistic approach, Int. J. Multiscale Comput. Eng. 16 (4) (2018) 367–376, doi:10.1615/IntJMultCompEng.2018026027.

[8] R. Watanabe, Possible slip systems in body centered cubic iron, Mater. Trans. 47 (8) (2006) 1886–1889, doi:10.2320/matertrans.47.1886.

[9] J. Christian, S. Mahajan, Deformation twinning, Prog. Mater. Sci. 39 (1-2) (1995) 1–157, doi:10.1016/0079-6425(94)00007-7.

[10] G. Monnet, D. Terentyev, Structure and mobility of the $\frac{1}{2}\langle 111\rangle\{112\}$ edge dislocation in bcc iron studied by molecular dynamics, Acta Mater. 57 (5) (2009) 1416–1426, doi:10.1016/j.actamat.2008.11.030.

[11] S. Queyreau, J. Marian, M.R. Gilbert, B.D. Wirth, Edge dislocation mobilities in bcc Fe obtained by molecular dynamics, Phys. Rev. B 84 (6) (2011) 064106, doi:10.1103/PhysRevB.84.064106.

[12] C. Woodward, S.I. Rao, *Ab-initio* simulation of isolated screw dislocations in bcc Mo and Ta, Philos. Mag. A 81 (5) (2001) 1305–1316, doi:10.1080/01418610108214442.

[13] G. Wang, A. Strachan, T. Çağin, W.A. Goddard III, Calculating the Peierls energy and Peierls stress from atomistic simulations of screw dislocation dynamics: application to bcc tantalum, Modelling Simul. Mater. Sci. Eng. 12 (4) (2004) S371, doi:10.1088/0965-0393/12/4/S06.

[14] X.-G. Li, C. Chen, H. Zheng, Y. Zuo, S.P. Ong, Complex strengthening mechanisms in the NbMoTaW multi-principal element alloy, npj Comput. Mater. 6 (2020) 70, doi:10.1038/s41524-020-0339-0.

[15] F. Ackermann, H. Mughrabi, A. Seeger, Temperature- and strain-rate dependence of the flow stress of ultrapure niobium single crystals in cyclic deformation, Acta Metall. 31 (9) (1983) 1353–1366, doi:10.1016/0001-6160(83)90006-8.

[16] H. Lim, C.R. Weinberger, C.C. Battaile, T.E. Buchheit, Application of generalized non-Schmid yield law to low-temperature plasticity in bcc transition metals, Modelling Simul. Mater. Sci. Eng. 21 (4) (2013) 045015, doi:10.1088/0965-0393/21/4/045015.

[17] S. Xu, Y. Su, Dislocation nucleation from symmetric tilt grain boundaries in body-centered cubic vanadium, Phys. Lett. A 382 (17) (2018) 1185–1189, doi:10.1016/j.physleta.2018.03.002.

[18] Z. Wang, C.T. Liu, P. Dou, Thermodynamics of vacancies and clusters in high-entropy alloys, Phys. Rev. Mater. 1 (4) (2017) 043601, doi:10.1103/PhysRevMaterials.1.043601.

[19] C. Lee, G. Song, M.C. Gao, R. Feng, P. Chen, J. Brechtl, Y. Chen, K. An, W. Guo, J.D. Poplawsky, S. Li, A.T. Samaei, W. Chen, A. Hu, H. Choo, P.K. Liaw, Lattice distortion in a strong and ductile refractory high-entropy alloy, Acta Mater. 160 (2018) 158–172, doi:10.1016/j.actamat.2018.08.053.

[20] F. Mompiou, D. Tingaud, Y. Chang, B. Gault, G. Dirras, Conventional vs harmonic-structured β-Ti-25Nb-25Zr alloys: A comparative study of deformation mechanisms, Acta Mater. 161 (2018) 420–430, doi:10.1016/j.actamat.2018.09.032.

[21] S.I. Rao, B. Akdim, E. Antillon, C. Woodward, T.A. Parthasarathy, O.N. Senkov, Modeling solution hardening in BCC refractory complex concentrated alloys: NbTiZr, $Nb_{1.5}TiZr_{0.5}$and $Nb_{0.5}TiZr_{1.5}$, Acta Mater. 168 (2019) 222–236, doi:10.1016/j.actamat.2019.02.013.

[22] B. Chen, S. Li, H. Zong, X. Ding, J. Sun, E. Ma, Unusual activated processes controlling dislocation motion in body-centered-cubic high-entropy alloys, Proc. Natl. Acad. Sci. USA 117 (28) (2020) 16199–16206, doi:10.1073/pnas.1919136117.

[23] S. Yin, J. Ding, M. Asta, R.O. Ritchie, Ab initio modeling of the energy landscape for screw dislocations in body-centered cubic high-entropy alloys, npj Comput. Mater. 6 (2020) 110, doi:10.1038/s41524-020-00377-5.

[24] F. Maresca, W.A. Curtin, Theory of screw dislocation strengthening in random BCC alloys from dilute to “High-Entropy” alloys, Acta Mater. 182 (2020) 144–162, doi:10.1016/j.actamat.2019.10.007.

[25] F. Wang, G.H. Balbus, S. Xu, Y. Su, J. Shin, P.F. Rottmann, K.E. Knipling, J.-C. Stinville, L.H. Mills, O.N. Senkov, I.J. Beyerlein, T.M. Pollock, D.S. Gianola, Multiplicity of dislocation pathways in a refractory multiprincipal element alloy, Science 370 (6512) (2020) 95–101, doi:10.1126/science.aba3722.

[26] A. Ghafarollahi, F. Maresca, W.A. Curtin, Solute/screw dislocation interaction energy parameter for strengthening in bcc dilute to high entropy alloys, Modelling Simul. Mater. Sci. Eng. 27 (8) (2019) 085011, doi:10.1088/1361-651X/ab4969.

[27] S. Ishibashi, Y. Ikeda, F. Körmann, B. Grabowski, J. Neugebauer, Correlation analysis of strongly fluctuating atomic volumes, charges, and stresses in body-centered cubic refractory high-entropy alloys, Phys. Rev. Mater. 4 (2) (2020) 023608, doi:10.1103/PhysRevMaterials.4.023608.

[28] S.I. Rao, C. Varvenne, C. Woodward, T.A. Parthasarathy, D. Miracle, O.N. Senkov, W.A. Curtin, Atomistic simulations of dislocations in a model BCC multicomponent concentrated solid solution alloy, Acta Mater. 125 (2017) 311–320, doi:10.1016/j.actamat.2016.12.011.

[29] F. Maresca, W.A. Curtin, Mechanistic origin of high strength in refractory BCC high entropy alloys up to 1900K, Acta Mater. 182 (2020) 235–249, doi:10.1016/j.actamat.2019.10.015.

[30] H. Lim, J.D. Carroll, J.R. Michael, C.C. Battaile, S.R. Chen, J.M. D. Lane, Investigating active slip planes in tantalum under compressive load: Crystal plasticity and slip trace analyses of single crystals, Acta Mater. 185 (2020) 1–12, doi:10.1016/j.actamat.2019.11.030.

[31] V. Vitek, M. Yamaguchi, Core structure of nonscrew $\frac{1}{2}\langle 111\rangle$dislocations on {110} planes in b.c.c. crystals. II. Peierls stress and the effect of an external shear stress on the cores, J. Phys. F: Met. Phys. 3 (3) (1973) 537–542, doi:10.1088/0305-4608/3/3/011.

[32] Y.N. Osetsky, D.J. Bacon, An atomic-level model for studying the dynamics of edge dislocations in metals, Modelling Simul. Mater. Sci. Eng. 11 (4) (2003) 427–446, doi:10.1088/0965-0393/11/4/302.

[33] D. Terentyev, D.J. Bacon, Y.N. Osetsky, Interaction of an edge dislocation with voids in α-iron modelled with different interatomic potentials, J. Phys.: Condens. Matter 20 (44) (2008) 445007, doi:10.1088/0953-8984/20/44/445007.

[34] M. Yamaguchi, V. Vitek, Core structures of non screw $\frac{1}{2}\langle 111\rangle$dislocations on {112} planes in b.c.c. crystals. II. Peierls stresses and the effects of an external shear stress on the cores, J. Phys. F: Met. Phys. 5 (1) (1975) 11–16, doi:10.1088/0305-4608/5/1/005.

[35] D. Terentyev, A. Bakaev, D.V. Neck, E.E. Zhurkin, Glide of dislocations in $\langle 111\rangle\{321\}$ slip system: an atomistic study, Philos. Mag. 96 (1) (2016) 71–83, doi:10.1080/14786435.2015.1126369.

[36] M.S. Duesbery, V. Vítek, D.K. Bowen, P.B. Hirsch, The effect of shear stress on the screw dislocation core structure in body-centred cubic lattices, Proc. R. Soc. Lond. A: Math. Phys. Eng. Sci. 332 (1588) (1973) 85–111, doi:10.1098/rspa.1973.0014.

[37] J. Marian, W. Cai, V.V. Bulatov, Dynamic transitions from smooth to rough to twinning in dislocation motion, Nature Mater. 3 (3) (2004) 158–163, doi:10.1038/nmat1072.

[38] J. Chaussidon, M. Fivel, D. Rodney, The glide of screw dislocations in bcc Fe: Atomistic static and dynamic simulations, Acta Mater. 54 (13) (2006) 3407–3416, doi:10.1016/j.actamat.2006.03.044.

[39] Y. Fan, Y.N. Osetsky, S. Yip, B. Yildiz, Onset mechanism of strain-rate-induced flow stress upturn, Phys. Rev. Lett. 109 (13) (2012) 135503, doi:10.1103/PhysRevLett.109.135503.

[40] A. Zunger, S.-H. Wei, L.G. Ferreira, J.E. Bernard, Special quasirandom structures, Phys. Rev. Lett. 65 (3) (1990) 353–356, doi:10.1103/PhysRevLett.65.353.

[41] A. van de Walle, P. Tiwary, M. de Jong, D.L. Olmsted, M. Asta, A. Dick, D. Shin, Y. Wang, L.Q. Chen, Z.K. Liu, Efficient stochastic generation of special quasirandom structures, Calphad 42 (2013) 13–18, doi:10.1016/j.calphad.2013.06.006.

[42] S. Xu, J.R. Mianroodi, A. Hunter, I.J. Beyerlein, B. Svendsen, Phase-field-based calculations of the disregistry fields of static extended dislocations in FCC metals, Philos. Mag. 99 (11) (2019) 1400–1428, doi:10.1080/14786435.2019.1582850.

[43] S. Xu, L. Smith, J.R. Mianroodi, A. Hunter, B. Svendsen, I.J. Beyerlein, A comparison of different continuum approaches in modeling mixed-type dislocations in Al, Modelling Simul. Mater. Sci. Eng. 27 (7) (2019) 074004, doi:10.1088/1361-651X/ab2d16.

[44] F. Maresca, D. Dragoni, G. Csányi, N. Marzari, W.A. Curtin, Screw dislocation structure and mobility in body centered cubic Fe predicted by a Gaussian Approximation Potential, npj Comput. Mater. 4 (2018) 69, doi:10.1038/s41524-018-0125-4.

[45] K. Kang, V.V. Bulatov, W. Cai, Singular orientations and faceted motion of dislocations in body-centered cubic crystals, Proc. Natl. Acad. Sci. USA 109 (38) (2012) 15174–15178, doi:10.1073/pnas.1206079109.

[46] S. Xu, Y. Su, I.J. Beyerlein, Modeling dislocations with arbitrary character angle in face-centered cubic transition metals using the phase-field dislocation dynamics method with full anisotropic elasticity, Mech. Mater. 139 (2019) 103200, doi:10.1016/j.mechmat.2019.103200.
[47] S. Xu, J.R. Mianroodi, A. Hunter, B. Svendsen, I.J. Beyerlein, Comparative modeling of the disregistry and Peierls stress for dissociated edge and screw dislocations in Al, Int. J. Plast. 129 (2020) 102689, doi:10.1016/j.ijplas.2020.102689.
[48] E. Bitzek, P. Koskinen, F. Gähler, M. Moseler, P. Gumbsch, Structural relaxation made simple, Phys. Rev. Lett. 97 (17) (2006) 170201, doi:10.1103/PhysRevLett.97.170201.
[49] S. Plimpton, Fast parallel algorithms for short-range molecular dynamics, J. Comput. Phys. 117 (1) (1995) 1–19, doi:10.1006/jcph.1995.1039.
[50] A. Stukowski, Visualization and analysis of atomistic simulation data with OVITO—the Open Visualization Tool, Modelling Simul. Mater. Sci. Eng. 18 (1) (2010) 015012, doi:10.1088/0965-0393/18/1/015012.
[51] S. Xu, E. Hwang, W.-R. Jian, Y. Su, I.J. Beyerlein, Atomistic calculations of the generalized stacking fault energies in two refractory multi-principal element alloys, Intermetallics 124 (2020) 106844, doi:10.1016/j.intermet.2020.106844.
[52] X.W. Zhou, R.A. Johnson, H.N.G. Wadley, Misfit-energy-increasing dislocations in vapor-deposited CoFe/NiFe multilayers, Phys. Rev. B 69 (14) (2004) 144113, doi:10.1103/PhysRevB.69.144113.
[53] D.-Y. Lin, S.S. Wang, D.L. Peng, M. Li, X.D. Hui, An *n*-body potential for a Zr-Nb system based on the embedded-atom method, J. Phys.: Condens. Matter 25 (10) (2013) 105404, doi:10.1088/0953-8984/25/10/105404.
[54] X.-G. Li, C. Hu, C. Chen, Z. Deng, J. Luo, S.P. Ong, Quantum-accurate spectral neighbor analysis potential models for Ni-Mo binary alloys and fcc metals, Phys. Rev. B 98 (9) (2018) 094104, doi:10.1103/PhysRevB.98.094104.
[55] L. Dezerald, D. Rodney, E. Clouet, L. Ventelon, F. Willaime, Plastic anisotropy and dislocation trajectory in BCC metals, Nature Comm. 7 (1) (2016) 1–7, doi:10.1038/ncomms11695.
[56] C.R. Weinberger, G.J. Tucker, S.M. Foiles, Peierls potential of screw dislocations in bcc transition metals: Predictions from density functional theory, Phys. Rev. B 87 (5) (2013) 054114, doi:10.1103/PhysRevB.87.054114.
[57] F. Shimizu, S. Ogata, H. Kimizuka, T. Kano, J. Li, H. Kaburaki, First-principles calculation on screw dislocation core properties in BCC molybdenum, J. Earth Simulator 7 (2007) 17–21.
[58] S. Zhao, Y.N. Osetsky, Y. Zhang, Atomic-scale dynamics of edge dislocations in Ni and concentrated solid solution NiFe alloys, J. Alloys Compd. 701 (2017) 1003–1008, doi:10.1016/j.jallcom.2017.01.165.
[59] B. Douat, C. Coupeau, J. Bonneville, M. Drouet, L. Vernisse, L. Kubin, Atomic-scale insight into non-crystallographic slip traces in body-centred cubic crystals, Scr. Mater. 162 (2019) 292–295, doi:10.1016/j.scriptamat.2018.10.032.
[60] B. Douat, J. Bonneville, M. Drouet, L. Vernisse, C. Coupeau, Low temperature atomic-scale observations of slip traces in niobium, Scr. Mater. 183 (2020) 81–85, doi:10.1016/j.scriptamat.2020.03.026.
[61] C.R. Weinberger, B.L. Boyce, C.C. Battaile, Slip planes in bcc transition metals, Int. Mater. Rev. 58 (5) (2013) 296–314, doi:10.1179/1743280412Y.0000000015.
[62] L.T.W. Smith, Y. Su, S. Xu, A. Hunter, I.J. Beyerlein, The effect of local chemical ordering on Frank-Read source activation in a refractory multi-principal element alloy, Int. J. Plast. (2020) 102850, doi:10.1016/j.ijplas.2020.102850.
[63] S. Xu, Y. Su, L.T.W. Smith, I.J. Beyerlein, Frank-Read source operation in six body-centered cubic refractory metals, J. Mech. Phys. Solids 141 (2020) 104017, doi:10.1016/j.jmps.2020.104017.
[64] Y. Su, S. Xu, I.J. Beyerlein, *Ab initio*-informed phase-field modeling of dislocation core structures in equal-molar CoNiRu multi-principal element alloys, Modelling Simul. Mater. Sci. Eng. 27 (8) (2019) 084001, doi:10.1088/1361-651X/ab3b62.
[65] W.-R. Jian, Z. Xie, S. Xu, Y. Su, X. Yao, I.J. Beyerlein, Effects of lattice distortion and chemical short-range order on the mechanisms of deformation in medium entropy alloy CoCrNi, Acta Mater. 199 (2020) 352–369, doi:10.1016/j.actamat.2020.08.044.
[66] Y.Y. Zhao, T.G. Nieh, Correlation between lattice distortion and friction stress in Ni-based equiatomic alloys, Intermetallics 86 (2017) 45–50, doi:10.1016/j.intermet.2017.03.011.
[67] Y.Y. Zhao, Z.F. Lei, Z.P. Lu, J.C. Huang, T.G. Nieh, A simplified model connecting lattice distortion with friction stress of Nb-based equiatomic high-entropy alloys, Mater. Res. Lett. 7 (8) (2019) 340–346, doi:10.1080/21663831.2019.1610105.
[68] Z. Wu, H. Bei, G.M. Pharr, E.P. George, Temperature dependence of the mechanical properties of equiatomic solid solution alloys with face-centered cubic crystal structures, Acta Mater. 81 (2014) 428–441, doi:10.1016/j.actamat.2014.08.026.
[69] D. Rodney, L. Ventelon, E. Clouet, L. Pizzagalli, F. Willaime, Ab initio modeling of dislocation core properties in metals and semiconductors, Acta Mater. 124 (2017) 633–659, doi:10.1016/j.actamat.2016.09.049.
[70] L.R. Owen, N.G. Jones, Lattice distortions in high-entropy alloys, J. Mater. Res. 33 (19) (2018) 2954–2969, doi:10.1557/jmr.2018.322.
[71] L.R. Owen, N.G. Jones, Quantifying local lattice distortions in alloys, Scr. Mater. 187 (2020) 428–433, doi:10.1016/j.scriptamat.2020.06.030.
[72] H. Song, F. Tian, Q.-M. Hu, L. Vitos, Y. Wang, J. Shen, N. Chen, Local lattice distortion in high-entropy alloys, Phys. Rev. Mater. 1 (2) (2017) 023404, doi:10.1103/PhysRevMaterials.1.023404.
[73] L. Zhang, Y. Xiang, J. Han, D.J. Srolovitz, The effect of randomness on the strength of high-entropy alloys, Acta Mater. 166 (2019) 424–434, doi:10.1016/j.actamat.2018.12.032.
[74] Q.-J. Li, H. Sheng, E. Ma, Strengthening in multi-principal element alloys with local-chemical-order roughened dislocation pathways, Nature Comm. 10 (1) (2019) 1–11, doi:10.1038/s41467-019-11464-7.
[75] R. Pasianot, D. Farkas, Atomistic modeling of dislocations in a random quinary high-entropy alloy, Comput. Mater. Sci. 173 (2020) 109366, doi:10.1016/j.commatsci.2019.109366.
[76] Y. Zeng, X. Cai, M. Koslowski, Effects of the stacking fault energy fluctuations on the strengthening of alloys, Acta Mater. 164 (2019) 1–11, doi:10.1016/j.actamat.2018.09.066.
[77] S. Lee, M.J. Duarte, M. Feuerbacher, R. Soler, C. Kirchlechner, C.H. Liebscher, S.H. Oh, G. Dehm, Dislocation plasticity in FeCoCrMnNi high-entropy alloy: quantitative insights from in situ transmission electron microscopy deformation, Mater. Res. Lett. 8 (6) (2020) 216–224, doi:10.1080/21663831.2020.1741469.
[78] D. Chen, L.L. Costello, C.B. Geller, T. Zhu, D.L. McDowell, Atomistic modeling of dislocation cross-slip in nickel using free-end nudged elastic band method, Acta Mater. 168 (2019) 436–447, doi:10.1016/j.actamat.2019.02.035.
[79] W.G. Nöhring, W.A. Curtin, Dislocation cross-slip in fcc solid solution alloys, Acta Mater. 128 (2017) 135–148, doi:10.1016/j.actamat.2017.02.027.
[80] W.G. Nöhring, W.A. Curtin, Cross-slip of long dislocations in FCC solid solutions, Acta Mater. 158 (2018) 95–117, doi:10.1016/j.actamat.2018.05.027.
[81] Q. Ding, Y. Zhang, X. Chen, X. Fu, D. Chen, S. Chen, L. Gu, F. Wei, H. Bei, Y. Gao, M. Wen, J. Li, Z. Zhang, T. Zhu, R.O. Ritchie, Q. Yu, Tuning element distribution, structure and properties by composition in high-entropy alloys, Nature 574 (2019) 223–227, doi:10.1038/s41586-019-1617-1.
[82] S.I. Rao, C. Woodward, T.A. Parthasarathy, O. Senkov, Atomistic simulations of dislocation behavior in a model FCC multicomponent concentrated solid solution alloy, Acta Mater. 134 (2017) 188–194, doi:10.1016/j.actamat.2017.05.071.
[83] W.G. Nöhring, W.A. Curtin, Design using randomness: a new dimension for metallurgy, Scr. Mater. 187 (2020) 210–215, doi:10.1016/j.scriptamat.2020.06.012.
[84] M.R. Fellinger, H. Park, J.W. Wilkins, Force-matched embedded-atom method potential for niobium, Phys. Rev. B 81 (14) (2010) 144119, doi:10.1103/PhysRevB.81.144119.
[85] D. Segall, T. Arias, A. Strachan, W. Goddard, Accurate calculations of the Peierls stress in small periodic cells, J. Comput.-Aided Mater. Des. 8 (2) (2001) 161–172, doi:10.1023/A:1020001527113.
[86] J.A. Moriarty, V. Vitek, V.V. Bulatov, S. Yip, Atomistic simulations of dislocations and defects, J. Comput.-Aided Mater. Des. 9 (2) (2002) 99–132, doi:10.1023/A:1026022602578.
[87] L.M. Hale, J.A. Zimmerman, C.R. Weinberger, Simulations of bcc tantalum screw dislocations: Why classical inter-atomic potentials predict {112} slip, Comput. Mater. Sci. 90 (2014) 106–115, doi:10.1016/j.commatsci.2014.03.064.
[88] T. Suzudo, T. Onitsuka, K.-i. Fukumoto, Analyzing the cross slip motion of screw dislocations at finite temperatures in body-centered-cubic metals: molecular statics and dynamics studies, Modelling Simul. Mater. Sci. Eng. 27 (6) (2019) 064001, doi:10.1088/1361-651X/ab235e.
[89] C. Woodward, S.I. Rao, Flexible *ab initio* boundary conditions: Simulating isolated dislocations in bcc Mo and Ta, Phys. Rev. Lett. 88 (21) (2002) 216402, doi:10.1103/PhysRevLett.88.216402.